

AD-A148 628

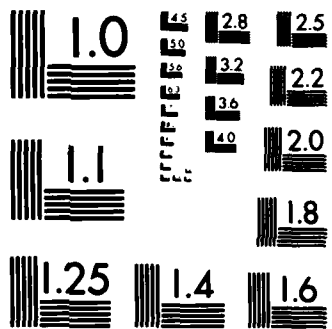
X RAYS FROM THE AURORA(U) AEROSPACE CORP EL SEGUNDO CA 1/1  
SPACE SCIENCES LAB P F MIZERA ET AL 30 SEP 84  
TR-0004(4478-32)-3 SD-TR-84-40 F04701-83-C-0084

UNCLASSIFIED

F/G 3/2

NL





MICROCOPY RESOLUTION TEST CHART  
NATIONAL BUREAU OF STANDARDS-1963-A

12

AD-A148 628

# X Rays from the Aurora

P. F. MIZERA and D. J. GORNEY  
Space Sciences Laboratory  
Laboratory Operations  
The Aerospace Corporation  
El Segundo, Calif. 90245

30 September 1984

DTIC FILE COPY

DTIC  
ELECTE  
DEC 14 1984  
S B D

APPROVED FOR PUBLIC RELEASE;  
DISTRIBUTION UNLIMITED

Prepared for  
SPACE DIVISION  
AIR FORCE SYSTEMS COMMAND  
Los Angeles Air Force Station  
P.O. Box 92960, Worldway Postal Center  
Los Angeles, Calif. 90009

84 12 06 016

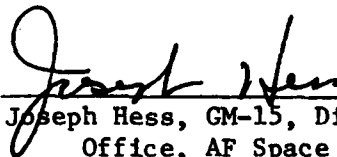
This report was submitted by The Aerospace Corporation, El Segundo, CA 90245, under Contract No. F04701-83-C-0084 with the Space Division, P.O. Box 92960, Worldway Postal Center, Los Angeles, CA 90009. It was reviewed and approved for The Aerospace Corporation by H. R. Rugge, Director, Space Sciences Laboratory. 1st Lt. Douglas R. Case, SD/YCM, was the Air Force project officer.

This report has been reviewed by the Public Affairs Office (PAS) and is releasable to the National Technical Information Service (NTIS). At NTIS, it will be available to the general public, including foreign nationals.

This technical report has been reviewed and is approved for publication. Publication of this report does not constitute Air Force approval of the report's findings or conclusions. It is published only for the exchange and stimulation of ideas.



Douglas R. Case, 1st Lt, USAF  
Project Officer -



Joseph Hess, GM-15, Director, West Coast  
Office, AF Space Technology Center

UNCLASSIFIED

SECURITY CLASSIFICATION OF THIS PAGE (When Data Entered)

REPORT DOCUMENTATION PAGE		READ INSTRUCTIONS BEFORE COMPLETING FORM
1. REPORT NUMBER SD-TR-84-40	2. GOVT ACCESSION NO.	3. RECIPIENT'S CATALOG NUMBER
4. TITLE (and Subtitle) X RAYS FROM THE AURORA	5. TYPE OF REPORT & PERIOD COVERED	
	6. PERFORMING ORG. REPORT NUMBER TR-0084(4478-32)-3	
7. AUTHOR(s) Paul F. Mizera and David J. Gorney	8. CONTRACT OR GRANT NUMBER(s)  FO4701-83-C-0084	
	9. PERFORMING ORGANIZATION NAME AND ADDRESS The Aerospace Corporation El Setundo, Calif. 90245	10. PROGRAM ELEMENT, PROJECT, TASK AREA & WORK UNIT NUMBERS
11. CONTROLLING OFFICE NAME AND ADDRESS Space Division Los Angeles Air Force Station Los Angeles, Calif. 90009	12. REPORT DATE 30 September 1984	
	13. NUMBER OF PAGES 16	
14. MONITORING AGENCY NAME & ADDRESS (if different from Controlling Office)	15. SECURITY CLASS. (of this report)  Unclassified	
	15a. DECLASSIFICATION/DOWNGRADING SCHEDULE	
16. DISTRIBUTION STATEMENT (of this Report)  Approved for public release; distribution unlimited.		
17. DISTRIBUTION STATEMENT (of the abstract entered in Block 20, if different from Report)		
18. SUPPLEMENTARY NOTES		
19. KEY WORDS (Continue on reverse side if necessary and identify by block number) Auroral remote sensing Ionospheric conductivity Ionospheric density X rays		
20. ABSTRACT (Continue on reverse side if necessary and identify by block number) Data from the x-ray instrument flown aboard the polar orbiting DMSP-F2 satellite are used to calculate electron distributions as inputs to energy deposition, electron density, and ionospheric conductivity computer codes. The calculated electron distributions are compared with those measured by the J-package instrument also aboard the satellite. A dawn-to-dusk auroral crossing during January 31, 1978 is used to provide the data from which		

DD FORM 1473 (FACSIMILE)

UNCLASSIFIED

SECURITY CLASSIFICATION OF THIS PAGE (When Data Entered)

UNCLASSIFIED

SECURITY CLASSIFICATION OF THIS PAGE(When Data Entered)

19. KEY WORDS (Continued)

20. ABSTRACT (Continued)

---the ionospheric parameters are calculated. The agreement between the two data sets is excellent and suggests that bremsstrahlung x rays can be used to remotely monitor ionospheric perturbations.

*... from remote sensing, and*

*...*

*f*

UNCLASSIFIED

SECURITY CLASSIFICATION OF THIS PAGE(When Data Entered)

CONTENTS

I. INTRODUCTION..... 3

II. EXPERIMENTAL TECHNIQUE..... 5

III. ANALYTICAL TECHNIQUE..... 7

IV. DISCUSSION..... 9

V. SUMMARY..... 17

REFERENCES..... 19

**S** DTIC  
 ELECTE **D**  
 DEC 14 1984  
**B**

Accession For	
NTIS GRA&I	<input checked="" type="checkbox"/>
DTIC TAB	<input type="checkbox"/>
Unannounced	<input type="checkbox"/>
Justification	
By	
Distribution/	
Availability Codes	
Dist	Avail and/or Special
A-1	



FIGURES

1a. Composite of Optical Imagery and Energy Deposition Rate Height Profiles from a Dawn Auroral Crossing by the DMSP-F2 Satellite on January 31, 1978. The profiles marked "electrons" use measured electron spectra while those marked "x rays" use electron spectra calculated from x rays..... 10

1b. Continuation of the Auroral Pass Shown in Fig. 1a over the Dusk Local-Time Region..... 11

2. Electron-Density Height Profiles from the Peak Deposition Rates from the Dawn and Dusk January 31, 1978 Auroral Crossing. The shaded region represents a typical mid-latitude density profile..... 13

3a. Hall and Pedersen Conductivities Calculated from the Dawn Density Profiles Shown in Fig. 2. The height-integrated conductivities are shown with the "x rays" values in parenthesis..... 15

3b. Same as Fig. 3a, but for the Dusk Auroral Crossing..... 16



## I. INTRODUCTION

Global magnetospheric-ionospheric coupling remains one of the most important topics in space research, particularly since the ionosphere can exert feedback on the magnetosphere. Energy and momentum input to the high-latitude ionosphere can alter global circulation of the atmosphere (Solar-Terrestrial Research for the 1980's, 1981).

The roles of ionospheric conductivity and Birkeland currents in regulating magnetospheric convection have been recognized for years, and recently conductivity and current measurements have been used to compute convection boundaries in magnetospheric models (Harel et al., 1981a and references therein). The conductivity of the ionosphere, particularly in the D and E regions at auroral latitudes, plays an important role in the formation of convection electric fields, Joule heating, particle precipitation, and auroral-charged particle acceleration. High-latitude Joule heating is an important source of energy for the thermosphere. However, good global estimates of Joule heating and conductivity are difficult to make with present observation techniques (Harel et al., 1981b), and monitoring of ionospheric parameters on a global scale, especially during magnetically active times, remains an important task in magnetospheric physics.

Remote sensing of ionospheric density perturbations resulting from precipitating 1-to-30-keV electrons can be accomplished by observing bremsstrahlung x rays from satellites. Pertinent ionospheric parameters can be computed by using electron spectra derived from bremsstrahlung x-ray observations.

## II. EXPERIMENTAL TECHNIQUE

The data were obtained from instruments aboard the USAF DMSP-F2 satellite (1977-044A), which was inserted in a nearly sun-synchronous polar orbit at an altitude of  $\approx 830$  km. The F2 satellite carried a low-energy auroral x-ray instrument, providing measurements in fifteen integral energy channels from 1.4 to 20 keV (see Mizera et al., 1978).

Precipitating electron fluxes in eight energy channels from 1 to 20 keV were measured each second by the J-package instrument. Images from the optical line scanning sensor, sensitive to light in the 475-to-750-nm region, were used to determine the longitudinal continuity of auroral forms away from the satellite ground track.

### III. ANALYTICAL TECHNIQUE

Terrestrial x-ray fluxes above a few keV observed at satellite altitudes are the result of magnetospheric electrons precipitating into the atmosphere. From the incident electron spectrum, pertinent ionospheric parameters such as ionization density and conductivity can be derived. One technique involving x-ray observations is to use their spectral characteristics to infer the incident precipitating electron spectrum. The inferred precipitating electron spectrum is then used as an input to a calculation of energy transport through the atmosphere, from which energy deposition rates and ionization rates can be determined as a function of altitude. Standard techniques exist for computing the altitude profiles of energy deposition, given an incident electron spectrum (Rees, 1963; Berger and Seltzer, 1972; Luhmann, 1977a), and techniques for determining the initial electron spectrum from observed x-ray spectra have also been discussed (e.g., Brown, 1971; Luhmann, 1977b; Walt et al., 1979).

We have applied the method described by Brown (1971) to infer incident electron spectra from observed DMSP bremsstrahlung x-ray spectra, even though some aspects of the method are not strictly appropriate for the earth's ionosphere. For example, atmospheric absorption and scattering of x rays are not treated in this calculation, even though the absorption effects might be significant for low-energy ( $\sim 1$  keV) x rays emitted at altitudes near 100 km. Brown's method basically involves the inversion of an integral relationship between the observed x-ray emission as a function of energy  $\phi(k)$  and the incident electron flux as a function of particle energy  $J(T)$ :

$$\phi(k) \sim \int_k^{\infty} Q(k,T) J(T) dT \quad (1)$$

where  $Q(k,T)$  is the bremsstrahlung cross section. If  $Q(k,T)$  takes the form of the Bethe-Heitler nonrelativistic formula for x-ray emission (neglecting Coulomb convections and shielding effects), whose energy dependence is of the form

$$q(k,T) = \frac{1}{kT} \log \frac{1+A}{1-A} \quad (2)$$

$$\text{where } A = \sqrt{1 - K/T}$$

then Eq. (1) can be inverted. The resulting expression for the incident electron spectrum takes the form

$$J(T) \sim T^2 \int_0^{\infty} \phi^1 [(1+x)K] g(x) dx \quad (3)$$

where  $\phi^1$  is a function involving the x-ray energy spectrum and its derivatives and  $g(x)$  is a polynomial weighting function [see Brown, 1971; Eqs. (8) through (12)].

Before the data from the DMSF x-ray instrument are applied to Eq. (3), they are temporally accumulated to assure a statistically significant spectrum ( $\sim 100$  counts in each energy channel). The accumulation interval is typically only 3 sec ( $\approx 20$  km) in active regions. The x-ray spectrum is logarithmically fit with a polynomial function of order  $n$  so that

$$n = \text{minimum}(4, m - 2) \quad (4)$$

where  $m$  is the number of "clean" data channels. At times, energy channels very near 3 keV are eliminated from the analysis because of obvious contamination by the argon  $K_{\alpha}$  emissions from the atmosphere.

The result is a logarithmic polynomial representing the incident-electron spectrum. This inferred electron spectrum is passed through an energy transport code (Luhmann, 1977a) that gives the energy deposition rate as a function of altitude. Relevant ionospheric parameters are calculated from this computed energy-deposition profile.

#### IV. DISCUSSION

January 31, 1978 was a magnetically disturbed day on the basis of the 3-hr Kp magnetic index ( $K_p \approx 4$  throughout the day). However, DMSP visible images from 10:30 to 21:00 hr UT indicate only moderate optical emissions.

Figure 1a shows a composite of the DMSP-F2 optical imagery and the calculated electron-energy deposition rates as the satellite crossed the dawn-to-midnight aurora. Midnight is on the upper right-hand corner of the photograph. The lower-latitude patchy aurora on the left is associated with peak electron fluxes in the few-keV energy range. Near the poleward boundary, the fluxes increase and approach 10 to 15 keV for their characteristic energy. On spatial scales of 100 km or so, electrons at energies less than 10 keV contribute mainly to the peak deposition rates. These characteristic electrons deposit their energy above 105 km in altitude.

In Figure 1a, the energy deposition rates labeled "electrons" are calculated by using 15-sec averages of precipitating 1-to-20-keV electron fluxes measured at the satellite. The deposition profiles labeled "x rays" are based on computed electron spectra using the techniques described in the preceding section. The peak deposition rates are  $\approx 700 \text{ keV/cm}^3\text{-sec}$ . Assuming the peak energy deposition occurs over a height of  $\sim 5 \text{ km}$ , the energy flux is  $\approx 0.7 \text{ ergs/sec-cm}^2$  at 105 km. Note that the calculated electrons from x rays mimic well the measured electrons for the main deposition peak and the satellite peaks.

Figure 1b shows data from the continuation of the auroral crossing on January 31, 1978. Midnight is near the upper left-hand corner of the photograph. Although the dusk visible auroral arcs in the premidnight sector are fainter than the dawn aurora, the energy deposition rates are larger by over a factor of two. The electrons associated with the dusk precipitation are also more energetic than in the dawn crossing. Electrons associated with the dusk arcs have peak fluxes near 13 keV, corresponding to peak deposition rates near 102 km altitude. Again, the spatial morphology of the deposition rates is almost one to one between x rays and electrons.

DMSP - F2  
JANUARY 31, 1978

DAWN  
AURORA

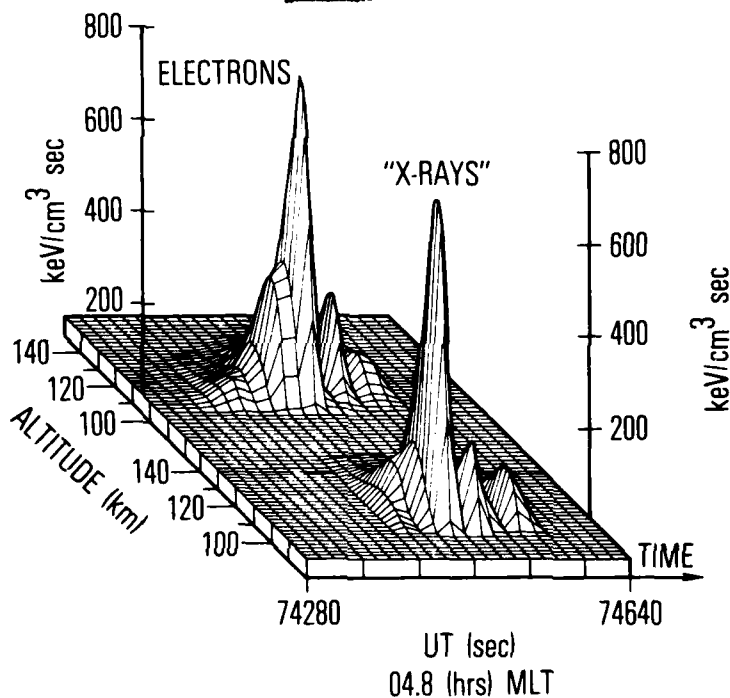


Fig. 1a. Composite of Optical Imagery and Energy-Deposition Rate Height Profiles from a Dawn Auroral Crossing by the DMSP-F2 Satellite on January 31, 1978. The profiles marked "electrons" use measured electron spectra, while those marked "x rays" use electron spectra calculated from x rays.

DMSP - F2

JANUARY 31, 1978

DUSK  
AURORA

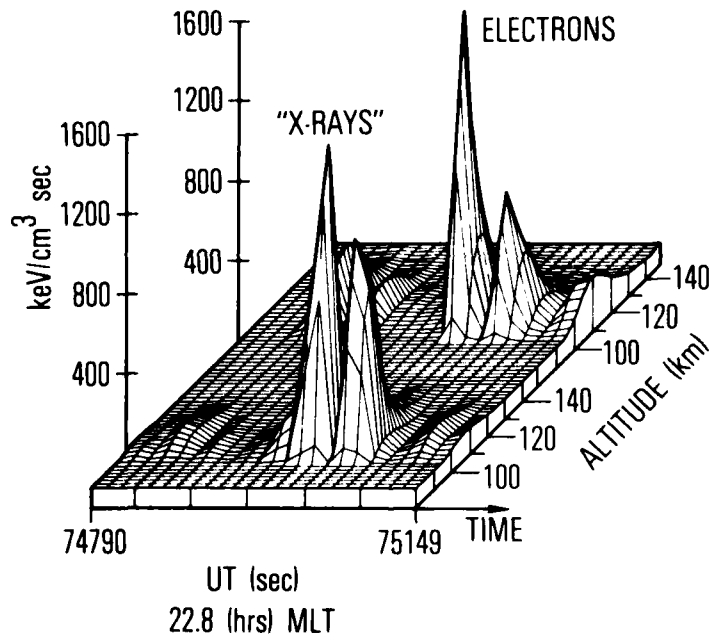


Fig. 1b. Continuation of the Auroral Pass Shown in Fig. 1a over the Dusk Local-Time Region.

In both the dawn and dusk crossings, the electron deposition profiles computed from the bremsstrahlung x rays are in excellent agreement with those calculated from the measured electrons. On the basis of these energy deposition rates, electron densities and conductivities are computed by using the standard techniques described earlier. Figure 2 shows the results of the calculation of the electron density height profile for the peak deposition rates during the dawn and dusk crossings on January 31, 1978. This calculation assumes that electron-ion pair production is balanced by recombination loss, so that the time derivative of the density is zero.

The solid line in Fig. 2 represents the calculation of density for the measured electron deposition, while the triangles show the density profile computed from the electron deposition calculated from the x-ray inversion technique for the dawn crossing. The dashed line and circles represent the densities for the measured and calculated electron spectra, respectively, for the dusk crossing. The calculations are for the peak deposition rates over each local-time crossing. The shaded profile represents a typical midlatitude density profile at night. This shows that the auroral zone densities can be well over an order of magnitude larger than adjacent regions.

The final quantities of interest are the electrical conductivities that are calculated from the electron densities. Again, standard techniques described earlier are used to determine the Pedersen and Hall conductivities.

Noting the good agreement between the calculated and measured electron densities in Fig. 2, we'd expect equally good agreement in the conductivity calculations. The only exception is for high altitudes ( $> 115$  km), where the electron spectra calculated from x rays are deficient at low energies ( $\sim 1$  keV). This might be due in part to the x-ray absorption described earlier. Atmospheric absorption of x rays is not treated in our spectral inversion calculation, and this absorption effect might be important in cases where electrons deposit their energy deep in the atmosphere, such as in the energetic dusk-sector event. A deficiency of low-energy x rays results in an underestimation of the lower-energy electron fluxes, which in turn produce a lower density at higher altitudes.



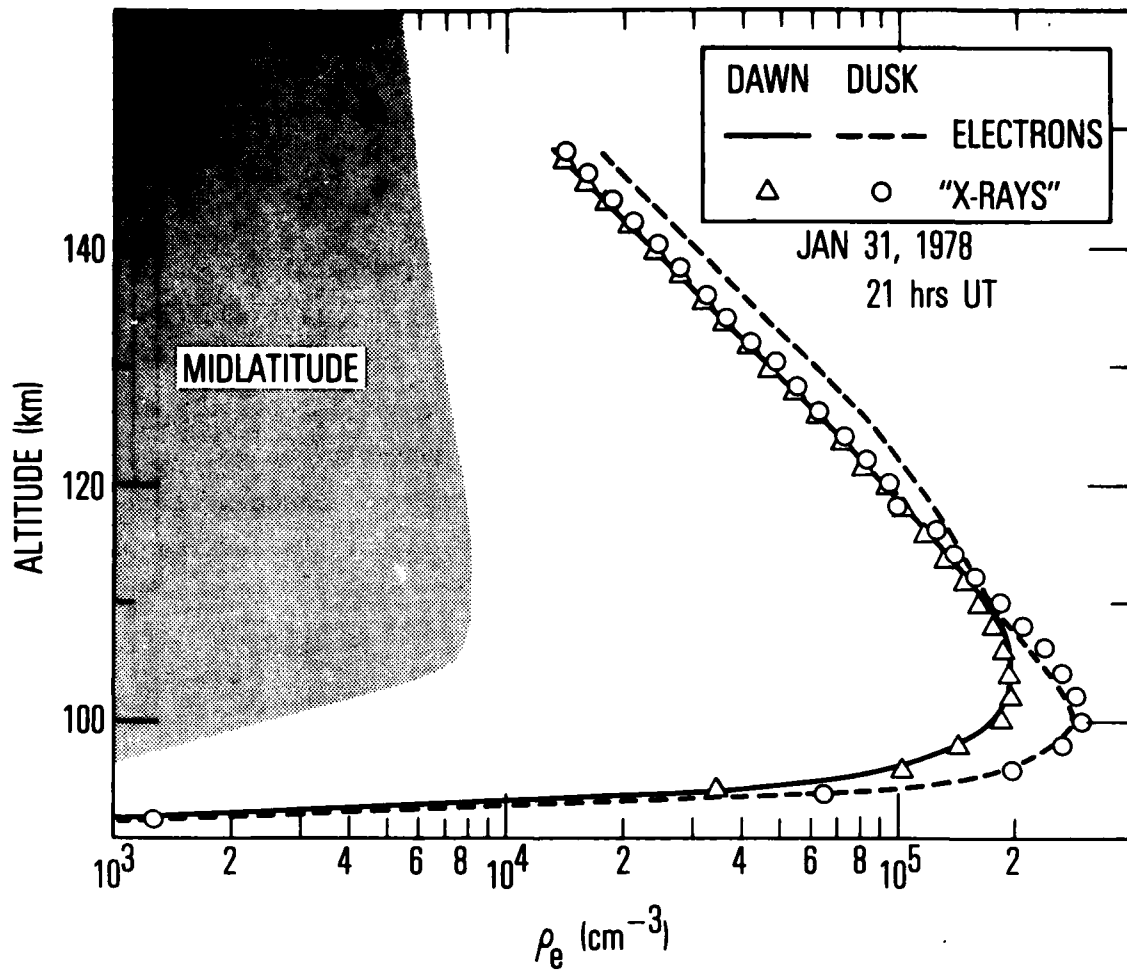


Fig. 2. Electron-Density Height Profiles from the Peak Deposition Rates from the Dawn and Dusk January 31, 1978 Auroral Crossing. The shaded region represents a typical midlatitude density profile.

Figure 3a shows the Pedersen and Hall conductivities as a function of altitude for the dawn aurora event on January 31, 1978. Again, the solid line represents calculations based on the measured electron spectrum, and the triangles represent those based on the inferred electron spectrum. The height-integrated conductivities ( $\Sigma_H$ ,  $\Sigma_P$ ) are also shown, with those in parenthesis representing the latter calculations. The Hall conductivity estimate is within 0.5% and the Pedersen conductivity is within 3% of the values computed directly from the measured electron spectrum.

Figure 3b shows the conductivity profiles and integrated conductivities for the dusk auroral crossing. The height-integrated Hall conductivity is 25% larger and the Pedersen conductivity is 20% larger in the dusk aurora than in the dawn aurora, as a result of the more energetic and intense electron precipitation in the dusk aurora. Again, the agreement between measured electron computed conductivities and inferred electron computed conductivities is excellent. (That is  $\approx 1.3\%$  for the Hall and  $\approx 7.3\%$  for the Pedersen.)

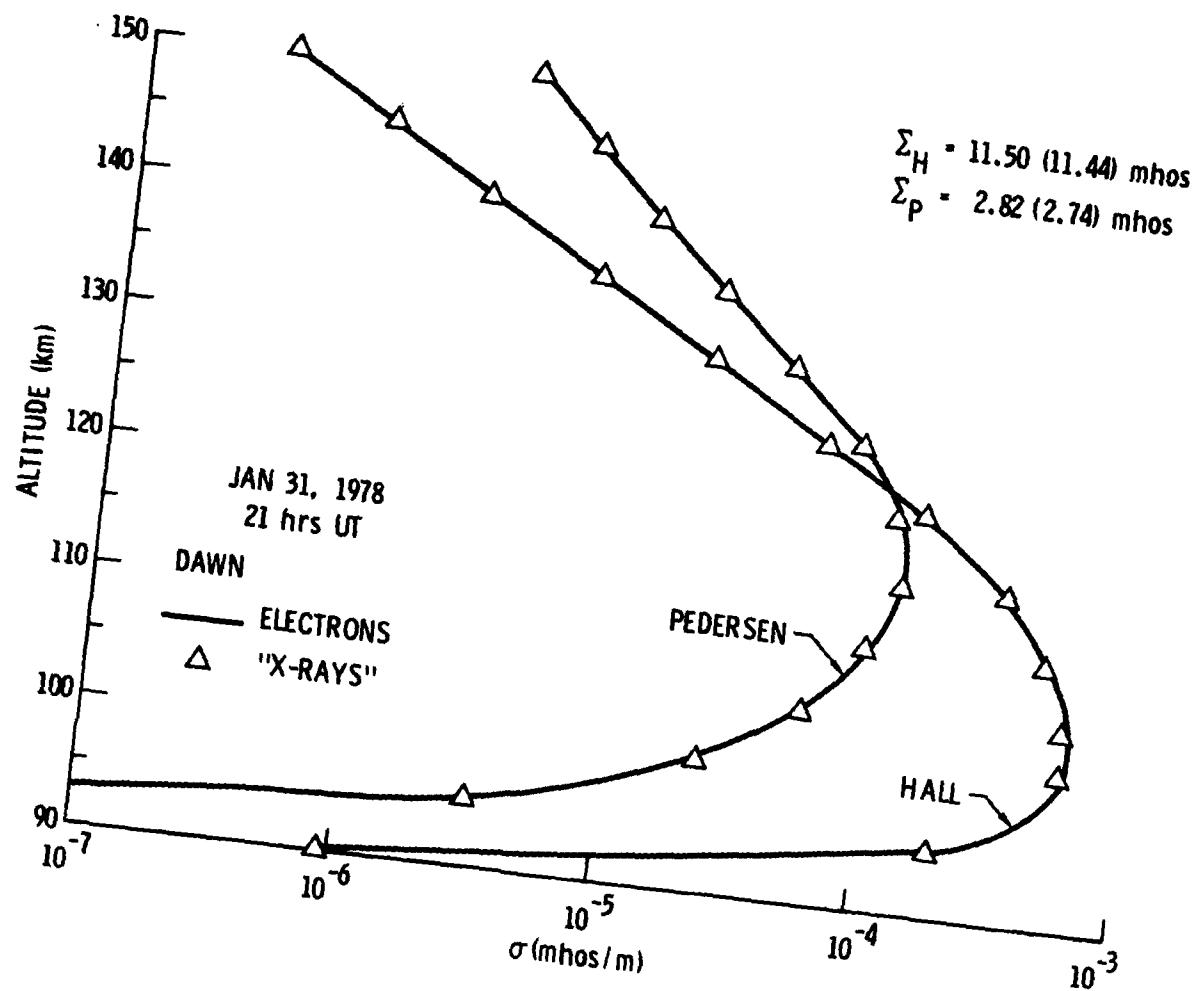


Fig. 3a. Hall and Pedersen Conductivities Calculated from the Dawn Density Profiles Shown in Fig. 2. The height-integrated conductivities are shown, with the "x rays" values in parenthesis.

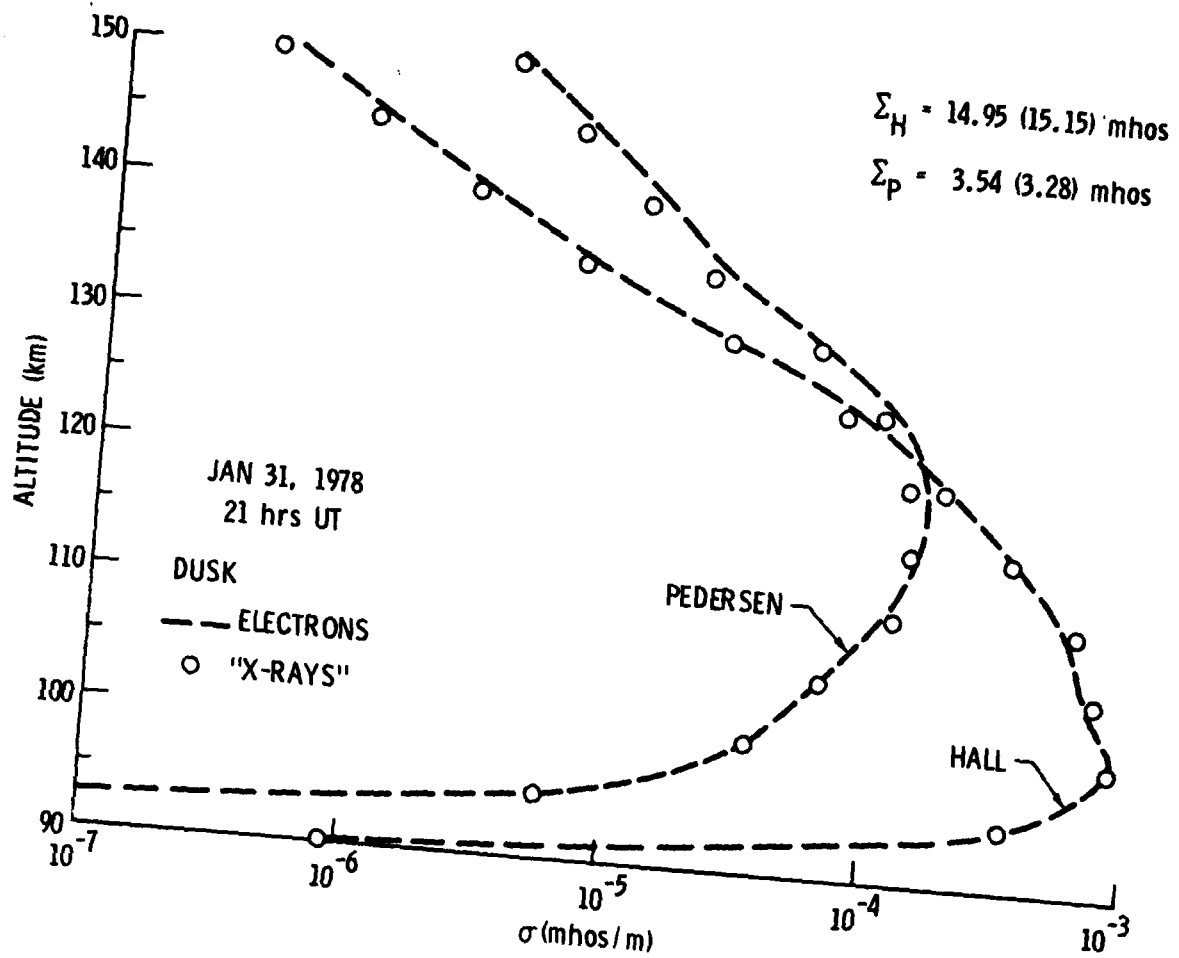


Fig. 3b. Same as Fig. 3a, but for the Dusk Auroral Crossing.

## V. SUMMARY

Data from the optical line scanner, the electron J-package instrument, and the low-energy x-ray sensor aboard the DMSP-F2 satellite show that remote sensing of precipitating electron spectra by bremsstrahlung x rays can provide useful ionospheric parameters such as electron densities and conductivities. The technique presently being used to calculate the electron spectra from x rays involves the inversion of the integral over the electron distribution and the bremsstrahlung cross section.

Examples from a typical dawn and dusk auroral crossing by the DMSP-F2 satellite provided sufficiently diverse electron spectral characteristics to test the agreement between measured and inferred electron spectra. There are, to be sure, some difficulties in using experimental data in the mathematical inversion. One such example was the deficiency of x rays generated in the lower-altitude atmosphere. Nevertheless, we have demonstrated that remote sensing of x rays can provide reasonably accurate quantities such as total energy, electron density, and conductivity in the E region of the auroral ionosphere.

Future endeavors involve different mathematical techniques to derive electron spectra from x rays. These include using a library of standard functions such as Gaussian, exponential, and Maxwellian distributions to represent the primary electron spectra. X-ray fluxes will be calculated and compared with the data and the distribution parameters will be varied for the best agreement.

The acquisition of the DMSP-F2 data was the first attempt to derive electron spectra by remote sensing. Since the x-ray instrument pointed along the nadir, only x rays emitted near the ground track were detected. The next generation of x-ray instruments, flown on the recently launched DMSP-F6, should provide global ionospheric parameters covering the high-latitude regions of the earth from limb to limb, nearly 2400 km across.

## REFERENCES

- Berger, M. J. and S. M. Seltzer, "Bremsstrahlung in the atmosphere," J. Atmos. Terr. Phys. 34, 85 (1972).
- Brown, J. C., "The deduction of energy spectra of non-thermal electrons in flares from the observed dynamic spectra of hard X-ray bursts," Sol. Phys. 18, 489 (1971).
- Harel, M., R. A. Wolf, P. H. Reiff, R. W. Spiro, W. J. Burke, F. J. Rich, and M. S. Smiddy, "Quantitative simulation of a magnetospheric substorm, 1. Model logic and overview," J. Geophys. Res. 86, 2217 (1981a).
- Harel, M., R. A. Wolf, P. H. Reiff, R. W. Spiro, W. J. Burke, F. J. Rich, and M. S. Smiddy, "Quantitative simulation of a magnetospheric substorm, 2. Comparisons with observations," J. Geophys. Res. 86, 2242 (1981b).
- Luhmann, J. G., "Auroral bremsstrahlung spectra in the atmosphere," J. Atmos. Terr. Phys. 38, 595 (1977).
- Luhmann, J. G., "Auroral electron spectra in the atmosphere," J. Atmos. Terr. Phys. 38, 605 (1977).
- Mizera, P. F., J. G. Luhmann, W. A. Kolasinski, and J. B. Blake, "Correlated observations of auroral arcs, electrons, and X-rays from a DMSP satellite," J. Geophys. Res. 83, 5573 (1978).
- Rees, M. H., "Auroral ionization and excitation by incident energetic electrons," Planet. Space Sci. 11, 1209 (1963).
- Solar-Terrestrial Research for the 1980's, Nat. Acad. Press, Geo. Res. Board, Washington, D.C. (1981).
- Walt, M., L. L. Newkirk, and W. E. Francis, "Bremsstrahlung produced by precipitating electrons," J. Geophys. Res. 84, 967 (1979).

## LABORATORY OPERATIONS

The Laboratory Operations of The Aerospace Corporation is conducting experimental and theoretical investigations necessary for the evaluation and application of scientific advances to new military space systems. Versatility and flexibility have been developed to a high degree by the laboratory personnel in dealing with the many problems encountered in the nation's rapidly developing space systems. Expertise in the latest scientific developments is vital to the accomplishment of tasks related to these problems. The laboratories that contribute to this research are:

Aerophysics Laboratory: Launch vehicle and reentry aerodynamics and heat transfer, propulsion chemistry and fluid mechanics, structural mechanics, flight dynamics; high-temperature thermomechanics, gas kinetics and radiation; research in environmental chemistry and contamination; cw and pulsed chemical laser development including chemical kinetics, spectroscopy, optical resonators and beam pointing, atmospheric propagation, laser effects and countermeasures.

Chemistry and Physics Laboratory: Atmospheric chemical reactions, atmospheric optics, light scattering, state-specific chemical reactions and radiation transport in rocket plumes, applied laser spectroscopy, laser chemistry, battery electrochemistry, space vacuum and radiation effects on materials, lubrication and surface phenomena, thermionic emission, photosensitive materials and detectors, atomic frequency standards, and bioenvironmental research and monitoring.

Electronics Research Laboratory: Microelectronics, GaAs low-noise and power devices, semiconductor lasers, electromagnetic and optical propagation phenomena, quantum electronics, laser communications, lidar, and electro-optics; communication sciences, applied electronics, semiconductor crystal and device physics, radiometric imaging; millimeter-wave and microwave technology.

Information Sciences Research Office: Program verification, program translation, performance-sensitive system design, distributed architectures for spaceborne computers, fault-tolerant computer systems, artificial intelligence, and microelectronics applications.

Materials Sciences Laboratory: Development of new materials: metal matrix composites, polymers, and new forms of carbon; component failure analysis and reliability; fracture mechanics and stress corrosion; evaluation of materials in space environment; materials performance in space transportation systems; analysis of systems vulnerability and survivability in enemy-induced environments.

Space Sciences Laboratory: Atmospheric and ionospheric physics, radiation from the atmosphere, density and composition of the upper atmosphere, aurorae and airglow; magnetospheric physics, cosmic rays, generation and propagation of plasma waves in the magnetosphere; solar physics, infrared astronomy; the effects of nuclear explosions, magnetic storms, and solar activity on the earth's atmosphere, ionosphere, and magnetosphere; the effects of optical, electromagnetic, and particulate radiations in space on space systems.

**END**

**FILMED**

**1-85**

**DTIC**